STOICHIOMETRIC, OPTICAL AND STRUCTURAL PROPERTIES EVOLUTIONS IN TiNx-Oy THIN FILMS PREPARED AT DIFFERENT REACTIVE SPUTTERING TIME

E. AJENIFUJA[a, b, c, *], A. P. POPOOLA[a], O. POPOOLA[b], A. Y. FASASI[c],
G. A. OSINKOLU[c], D. A. PELEMO[c], E. I. OBIAJUNWA[c]
[a]Department of Chemical, Metallurgical and Materials Engineering, Tshwane University of Technology, Pretoria, South Africa
[b]Centre for Energy and Electric Power, Tshwane University of Technology, Pretoria, South Africa
[c]Center for Energy Research and Development, Obafemi Awolowo University, Ile-Ife, Nigeria

Formation of titanium oxynitride at relative low sputtering pressure ($\leq$ 9.98 E-3 Torr) in reactive nitrogen and residual oxygen atmosphere has been observed from previous experiments. In the present study, TiNx-Oy thin film samples with varied thickness, composition and morphology were grown at a fixed low sputtering pressure (8.03E-3 Torr) on glass substrates from 99.99 % purity titanium target, nitrogen gas and vacuum residual oxygen at 200 W. The stoichiometry and thickness variations were studied by Rutherford backscattering (RBS) spectrometry, while X-ray diffractometry (XRD), scanning electron microscopy and UV-Visible spectrophotometry were used to study the structural and optical characteristics of the films. Stoichiometric changes with increase N/Ti and N/O ratios in the films were observed with sputtering time and thickness. Increase in crystallinity with film thickness was seen with preferred orientation at (111) attributed to α-Ti. The films transmission onset red-shift towards visible region with thickness with % Tmax of 14.273 at 574 nm wavelength. The bandgap values varied from 3.72 eV to 2.81 eV with increase in the film thickness.

1. Introduction

Transition-metal oxynitrides are special class of materials that may exhibit properties of both oxides and nitrides. For instance, it is possible to vary the bandgap, structure, and the optoelectronic properties of TiNxOy by altering the nitride/oxide (N/O) ratio [1-3], which is a significant reason for their wide applications. Now, advances are being made in titanium oxynitride research in optoelectronics, photonics, surface protection and in some other fields i.e. photocatalysis, and water splitting processes for hydrogen release. If the bandgap in TiNxOy is narrowed, it could lead to enhanced activity in the visible light range [4-6]. With the possibility of bandgap tuning via N/O or N/Ti ratio variation, titanium oxynitride could also be used as a wide band gap (WBG) materials. WBG materials are semiconductors with a relatively large band gap compared to a typical semiconductor (1-1.5 eV). Their bandgap fails in the range of 2 - 4 eV [7, 8]. WBG property is particularly important for allowing devices to operate at much higher temperatures, on the order of 300 °C. Accordingly, this makes them highly promising for military applications and in new electrical grid and alternative energy devices. TiNxOy possess good structural and optical characteristics, which could make them useful for narrow and wide bandgap applications. Metal oxynitrides have been observed to be more stable in air and moisture than pure nitrides due to already oxygen presence [9-11], and this could lead to useful surface oxidation and corrosion resistance qualities.

---

[*]Corresponding author: eajenifuja@gmail.com

Titanium oxynitrides are synthesized in different forms such as thin films and nanoparticles depending on the anticipated application. Most metal oxynitrides are prepared as thin films on suitable substrates and they often exhibit unique dual oxide-nitride properties, and titanium oxynitride has been one of the most intensively studied systems. Findings have shown that these compounds exhibit a complex structure with intermediate characteristics between metallic TiN and insulating TiO_2 thereby simultaneously exhibiting high hardness and wear resistance with good optical and electrical properties [12-14]. Optoelectronic application of TiN_xO_y thin films is particularly dependent on N/O ratio [1, 4, 6]. For instance, oxygen-rich TiN_xO_y films are used as insulating layers in metal-insulator-metal (MIM) capacity structures, while diffusion barriers utilizes nitrogen-rich TiN_xO_y [14, 15]. The stoichiometric ratio of TiN_xO_y films should be carefully controlled and properly assessed in order to be effective for utilization. Difficulties in achieving targeted N/O ratio in titanium oxynitride thin films have been reported in several studies [14-18]. Techniques such as water and reactive gas pulsing have been used in studies to vary N/O ratio in TiN_xO_y films [12, 19, 20]. Braic et al., [14] utilized different levels of chamber residual oxygen to synthesize TiN_xO_y films of varied optical properties. In sputtering, titanium oxynitrides are usually fabricated by mixture of inert argon, and reactive nitrogen and oxygen gases in an evacuated chamber containing pure Ti target. More understanding on structural, stoichiometry and optical properties of TiNO thin films in relation to both N/Ti and N/O ratios is important for appropriate design. Ti_2N with metallic nature is considered promising for new areas of interest and application [21-23].

In this study, TiN_x-O_y thin films with range of stoichiometry, optical and structural properties were prepared at different sputtering time in an optimized sputtering pressure condition using nitrogen residual oxygen reactive gas mixture. Hence, the background residual oxygen was solely used as the oxygen ions source. We report herein, the evolution in the stoichiometry, N/Ti and N/O ratios, with thickness using Rutherford backscattering spectrometry (RBS). Optical and structural analysis results are also presented with respect to the thickness and compositions.

2. Experimental procedure

TiN_x-O_y thin films on soda lime glass substrates were prepared by reactive magnetron sputtering. A stainless-steel chamber was evacuated with turbo-molecular pump backed by a mechanical pump down to a base vacuum close of 9.98 E-6 Torr, before the release of the argon and nitrogen. The substrates were prepared by rinsing sequentially with methanol, acetone, de-ionized water and 20% HNO_3 to remove dust and oily layer on the surface and then dried using nitrogen gas. For plasma generation, high purity argon was used and the sputtering target was a 99.99% pure Ti disc (5 mm thick and of 50.8 mm diameter) fixed at an angle of about 45° relative to the static substrate platform. Pre-sputtering cleaning for Ti target was carried out in a pure argon atmosphere, with the shutter positioned shield the substrates from plasma flow the target. Thereafter high purity nitrogen gas was released into the chamber via the control valve to initiate reactive sputtering. The parameters used for the preparation of TiN_x-O_y films are given in Table 1. The deposition chamber was left to cool to the room temperature before the films were removed. Ion beam analysis (IBA) of the samples was done using NEC 5SDH 1.7 MeV Pelletron Tandem Accelerator, equipped with an RF charge exchange ion source to provide proton and helium ions.

The measurement using the Rutherford backscattering spectrometry was performed using the $^4He^+$ ion beam and the incident energy was 2.2 MeV with the detector energy resolution of 12.0 KeV. The RBS spectra were recorded and the data obtained were fitted to determine the stoichiometry, thickness and compositional depth profile of the films. The crystallographic analysis was done with MD-10 Precision X-Ray Diffractometer with 2 theta angles between 16° and 72° using CuKα radiation. X'Pert High Score and Profex, x-ray diffraction analysis softwares were used to study and determine the crystallographic parameters [24]. Scanning electron microscope (Carl Zeiss MA-10 SEM) and optical microscope were used to analyze the morphology and the microstructure of the films. Optical characteristics of the films were determined from transmission measurements using a UV-Visible spectrophotometer (Thermo Scientific Helios Omega) with the wavelength (λ) ranging from 200 to 1100 nm. The acquired data

was used to generate the normalized transmittance in order to have a better picture of the relative absorption edge as it changes with film thickness.

Table 1. Sputtering parameters for TiNx-Oy thin films on glass substrates

Item	Values
Substrate	Sodalime glass (75 x 26 x 1 mm)
Reactive gases	Nitrogen, Oxygen (Residual)
Sputtering gas	Argon
Power	200
Sputtering Time	5 – 25 minutes
Base Pressure	9.98 E-6 Torr
Sputtering Pressure	8.03 E-3 Torr

3. Results and discussions

3.1. Thickness and stoichiometry analysis

The RBS data for the sputtered TiNx-Oy samples were obtained using 2.2 MeV ^{4}He$^+$ ions, and they were analyzed using the SIMNRA 6.06 code [25]. The selected spectra of the films are shown in Figs. 1(a) – (d). Rutherford backscattering method simultaneously provided information about the areal density (RBS thickness) and stoichiometry of the films, while depth profile data of the layers was also extracted. SIMNRA software was used to correctly fit the simulation over experimental data and gave the required information regarding the samples. Both the heavy element Ti, and the light elements (N and O) were detected via the backscattering process. Remarkable amount of oxygen was detected in samples sputtered at low deposition time TON-05 (5 minutes) and TON-10 (10 minutes) (detail in Table 2), and this was also confirmed visually from the characteristic dark blue colour of titanium oxynitrides. The changes in films thickness can be seen from the width of corresponding Ti peaks. The film thickness was obtained in RBS unit (10^{15} atoms/cm^2), and the effective compositions of the sputtered films at different time are given in Table 1. The variations in colour of the films were noticed depending on the thickness, and it also signified variations in film compositions. The colour observed agrees with recent studies [14, 26-27]. Braic et al. [14] showed the effect of residual oxygen level on the optical properties of sputtered titanium oxynitride thin films. In the study [14], TiNxOy samples sputtered under high residual oxygen level exhibited non-metallic (TiO$_2$) behaviour, while the films sputtered at low level of residual oxygen showed a metallic (TiN) behaviour. However, in this study, the experiments are based on earlier optimized sputtering pressure conditions [27-28]. The same residual oxygen level is assumed for each experiment, since a constant base pressure conditions was attained before each sputtering. Hence, the fixed residual oxygen level in the evacuated chamber was systematically reduced by increasing the sputtering time from 5 to 25 minutes for each subsequent experiment. Meanwhile, since there would be an initial interplay between the oxygen and nitrogen content, the sputtering time would also affect the nitrogen content and the sputtering mode [29]. This is conspicuous from the stoichiometric analysis, the films sputtered at lowest deposition time contained highest amount of oxygen, which indicated relatively higher background residual oxygen, while the TiNx-Oy film samples prepared at 25 minutes contain negligible amount of oxygen. The sputtering conditions adopted allowed simultaneous, but controlled variation in the thickness and compositional profile of the films. The RBS thickness and the effective stoichiometry of the sputtered TiNx-Oy films on glass substrates are shown in Table 2. Studies have shown that the most active material at very low sputtering pressure is the ionized target atoms, which is when the atomic emission of titanium is strong, and increasing the sputtering pressure, will result in the increase of fractional flow of nitrogen [27, 29-31]. In this work, nitrogen ion is observed to dominate with increase in sputtering time, due to the damping residual oxygen and the effect of its constant fractional flow on the sputtering mode, changing from oxide to nitride mode. From the relationship shown in Fig. 2, nitrogen ions emission intensity was increasing against both titanium and oxygen. A steady increase in the N/O and N/Ti ratios was

seen in the films, which indicated a sustained change in the compositions with thickness. Also, the degree of filling of the non-metallic sub-lattice in nitrides has been shown to increase linearly as the nitrogen content rises [32-33]. Herein, it is shown that change in sputtering time induced an overall change in composition of the films from oxynitride phase (TiNxOy) to sub-stoichiometric nitride phase (Ti$_2$N). From the trend of N/Ti plot (Fig. 2) an indication is shown of a steady move towards stoichiometric TiN (N/Ti = 1) as sputtering time increases, with resultant increase in film thickness.

Table 2. Elemental composition and RBS thickness values of the film on glass substrates

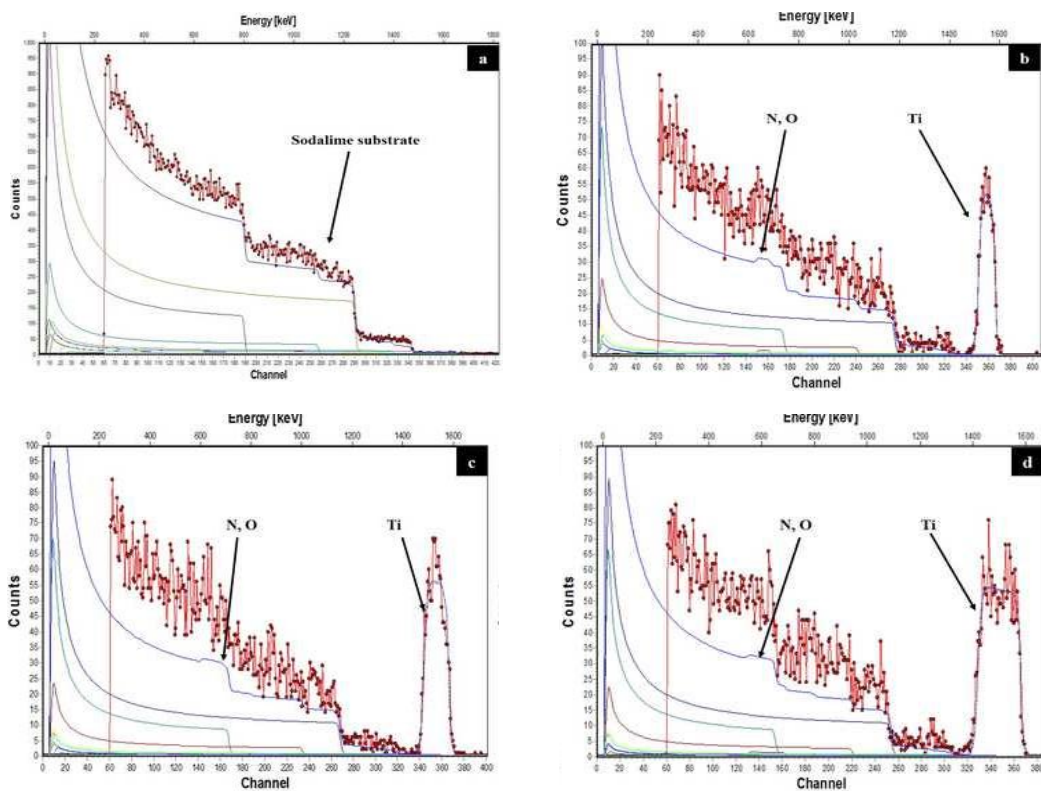| Sample	Deposition time (minute)	RBS (1015 atoms/cm^2)	Elemental Compositions (100%)		
			Ti	N	O
TON-05	5	655.085	0.735	0.143	0.122
TON-10	10	930.729	0.723	0.204	0.073
TON-15	15	1547.253	0.693	0.255	0.052
TON-20	20	2607.366	0.660	0.328	0.012
TON-25	25	3103.178	0.652	0.337	0.011

Fig. 1. RBS Spectra for the TiNx-Oy on soda lime glass substrates (a) Glass, (b) TON-05, (c) TONGL10, and (d) TON-GL15.
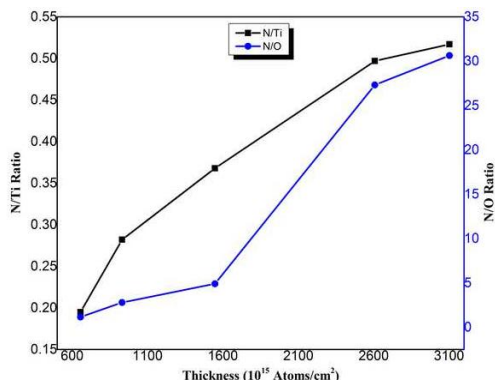
Fig. 2. Plots of N/O and N/Ti ratios as a function of TiNx-Oy thickness.

3.2. Optical properties

The thickness of the sputtered films was obtained in RBS unit (10^{15} Atoms/cm^2) using SIMNRA code, and the values were from 655.085 to 3103.178 (10^{15} Atoms/cm^2). The mass density of the sputtered films is not known and the area density might not be converted directly. However, with low oxygen content, the effective compositions of the thin films are observed to be closer to the stoichiometry of Ti_2N or NTi_2 [23, 27]. Therefore using the known mass density of TiN or TiO_2 could give a bad model for the atomic density (Atoms/cm3) determination of the sputtered films. Hence, assuming deliberately, the density of Ti_2N (4.91 g/cm^3) for the deposited films, a factor of 0.3711 was obtained for the conversion of sputtered TiNx-Oy films area densities (10^{15} Atoms/cm^2) into nanometer (nm) units, using the relation (Eq.1) given by Chu et al. [34]. Converting from areal density to (linear) thickness, the estimated values are given in Table 3, from 243.10 to 1151.59 nm. The linear thickness was obtained specifically for the estimation of the optical properties of the films. Percent and normalized transmittance spectra of the sputtered films are shown in Fig. 3. Expectedly, the transmittance (%T) of the TiNx-Oy films decreases with increasing sputtering time and nitrogen content, and this agrees with recent studies [31, 35]. It is observed from Fig. 3(b) that the absorption edges shift towards higher wavelength with increase in film thickness and N/Ti ratio. Therefore, it is evident from the transmission onset shift that the optical properties of the sputtered films do not only depend on thickness, but also on the nitrogen concentrations. The optical bandgap was determined from the absorption coefficient (a) using the Tauc relation (Eq. 2) [36].

$$Thickness = \frac{Atoms\ per\ unit\ area}{Atomic\ Density} \left(\frac{cm^{-2}}{cm^{-3}} \right)$$

(1)

$$\alpha h v = B \left(h v - E_g \right)^m$$

(2)

An extrapolation of the linear region of a plot of $(\alpha hv)^2$ versus photon energy (hv) gives the values of optical bandgap Eg. The bandgap energy spectra at different sputtering conditions are shown in Fig. 4(a) and (b), while the values are stated in Table 2. The energy gap values for the sputtered TiNx-Oy films ranged from 2.81 to 3.72 eV, which indicated, and as depicted in Fig. 5 (a) that films bandgap energy decrease steadily with thickness but increase with transmittance. The shift of the absorption edge towards higher wavelength is due to narrowing or thinning of the bandgap. As seen, the relationship between the optical bandgap and the N/O and N/Ti ratios (Fig. 5b) confirms evolution of the films from oxynitride (non-metallic) to nitrides (metallic) film, with compositions tending towards stoichiometric TiNx (x=1). Changes in Eg values can be attributed to the structural and compositional changes brought about by the formation of near-stoichiometric Ti_2N phases in the films at higher sputtering time and thickness. The formation of Ti_2N with metallic properties [14, 23] in the films may have localized some states in the deep energy levels, and hence lower the bandgap energy [37]. The observed bandgap evolution with thickness is in

strong agreement with recent studies [38-39]. The bandgap tuning is the re-ordering or refinement of the crystal structure, with changes in the atomic distance, grain size and structural defects [40]. For instance, electron-electron and electron-impurity scattering phenomenon usually observed in semiconductor as a bandgap shift, known as Moss-Burstein effect [30].
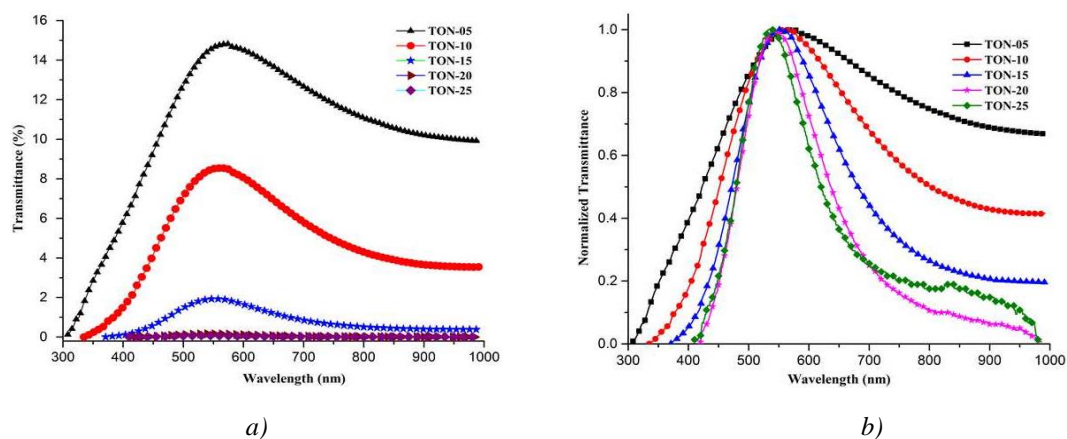

a)   *b)*

Fig. 3. (a) Percent transmittance and (b) normalized transmittance of the films at different sputtering time and thickness.

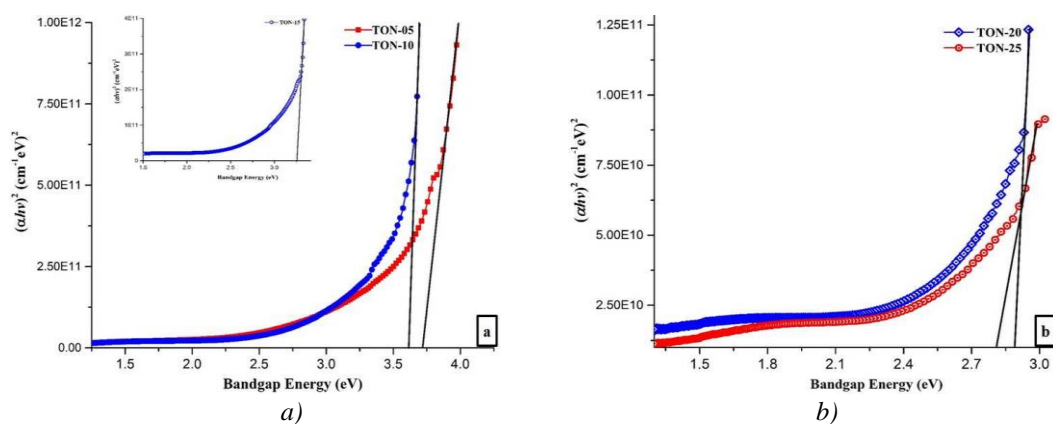*a)*   *b)*

Fig. 4. Bandgap energy plots for the TiOxNy samples (a) TON-05, 10, 15 and (b) TON-20, 25.

Table 3. Optical property values of TiNx-Oy films at different thicknesses.

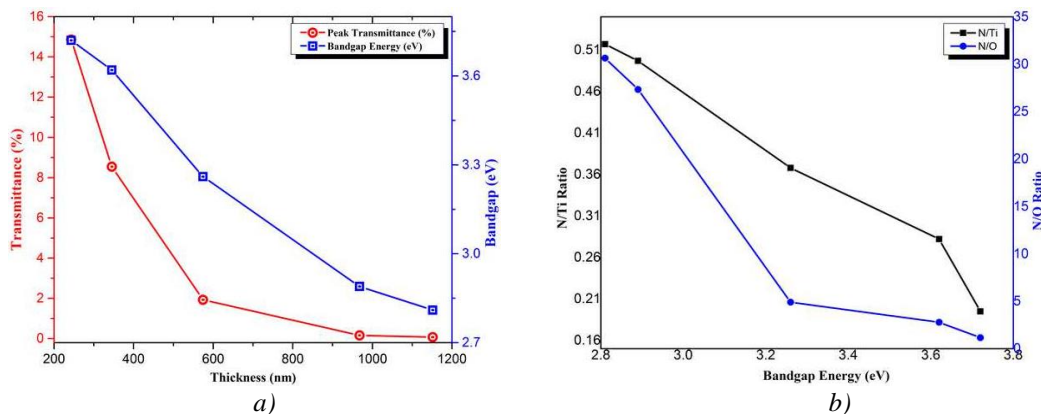| Sample	Thickness (nm)	Peak Transmittance (%)	Peak Wavelength (nm)	Bandgap (eV)
TON-05	243.10	14.861	574	3.72
TON-10	345.39	8.542	562	3.62
TON-15	574.19	1.932	554	3.26
TON-20	967.59	0.159	541	2.89
TON-25	1151.59	0.074	537	2.81

Fig. 5. TiNx-Oy thin films optical-structural relationships (a) variation in thickness with bandgap, (b) variation in bandgap with N/Ti and N/O ratios.

3.3. X-Ray diffraction analysis

X-ray diffraction spectra of the TiNx-Oy thin film samples are shown in Fig. 6. It is seen that film sample TON-05 with lowest thickness did not show any identifiable diffraction peak(s), but the next sputtered sample TON-10 showed a small bump which could indicate an onset of structural re-ordering of the detected crystalline phase with higher thickness. The absence of well-defined peak(s) in TON-05 spectrum makes it more to be regarded as amorphous. The amorphous properties exhibited by sample TON-05 is attributed to the substrate nature (soda lime glass). The crystallinity of deposited films is usually determined by the complex interaction between the substrate and the developing film [41-42]. At early stage of the film formation, the microstructure is related to the nucleation and growth in random orientations influence by the substrate. It is noted that, the thicker the TiNx-Oy films, the lower the influence of the amorphous glass substrate surface on its structural formation. Meanwhile, the sputtered films with thickness of 574.19 nm and above showed a sharp peak at about 40º (2θº) with preferred reflection at (111) attributed to α-Ti [43-45]. Stoichiometry variations in thin films often lead to changes in crystal structure, chemical bonding and free electron concentration. Hence, the main sources of non-stoichiometry in the sputtered TiNx-Oy films is the anion vacancies (x<1). The crystallographic behaviour follows the composition and optical results which indicated transition from non-metal (oxynitride) to metal-like (Ti$_2$N) characteristics. The film crystallographic parameters are shown in Table 4. The peak intensity is noted to change remarkably with thickness of the films. Based on the Debye-Scherer equation [46], the average crystallite (D) from the XRD peak width (βhkl) can be calculated using the following equation (3):

$$D = \frac{K * \lambda}{\beta_{hkl} \, Cos\,(\theta)}$$

(3)

where K = 0.94 is the shape factor approximately equal to unity. λ is the wavelength (1.5406 A˚ for CuKα radiation) and βhkl is the full width at half maximum (FWHM). The deduced values of crystallite size are presented in Table 4. It is assumed as the crystallite size of coherently diffracting domain, and may not necessarily be the same as the particle size. It is observed the crystallite size increased slightly with thickness. The crystallite size values conform to the optical characteristics of the sputtered films, which showed reduction and red shift of transmittance onset with film thickness. The larger the crystallites, the more the photon scattering and absorption at the surface and within the material.

Table 4. XRD data for the TiOxNy thin films on glass substrate at different thickness

Sample	Interplanar spacing, d(Å)	Lattice parameters, a, c (Å)		Orientation angle (2θ°)	FWHM (2θ°)	Crystallite size (nm)
TON-GL10	2.278	3.002	4.725	40.470	1.0412	8.49
TON-GL15	2.222	2.920	4.661	40.345	0.9011	9.81
TON-GL20	2.302	3.061	4.648	40.172	0.9830	8.99
TON-GL25	2.238	2.934	4.729	40.275	0.8413	10.50
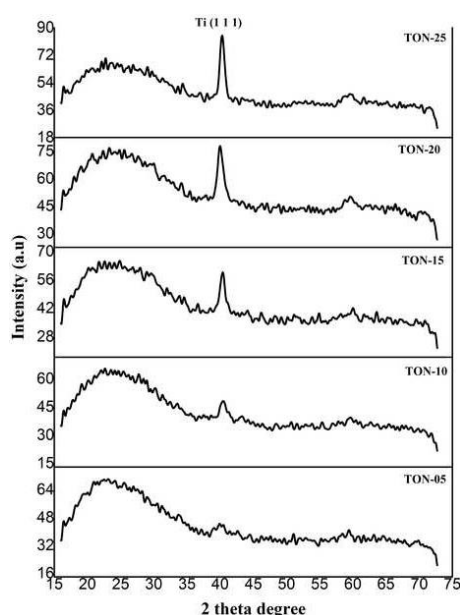
Fig. 6. XRD Spectra for the TiOxNy films on soda lime glass substrates at different thickness.

3.4. Surface microstructure

Scanning electron microscopy images of the film samples are shown in Figs. 7(a) and (b) for low thickness samples TON-05 and TON-10 respectively, while Fig. 7(c) shows the image for sample TON-20 with relative high thickness (967.59 nm). The images for the films deposited at lower sputtering time did not show much detail about the microstructural features at higher magnifications beyond present value, which might be the effect of the film surface properties and the non-conducting nature of substrates. As shown in the micrographs, there is a prior formation of smooth background layer, before accumulation of larger crystallites to form more layers. Highly dispersed rounded pores are observed to be distributed within the thinner films prepared at low sputtering time, meanwhile the representative image shown for high sputtering time (20 minutes) indicated tightly packed granular and uniformly shape microstructures on the dense background. The clear variation in the morphologies of the sputtered films can be attributed to the changes thickness of the films. The morphologies observed for sputtered films based on their thickness are in agreement with crystallographic results. At lower sputtering time (i.e. 5 mins), the impinging sputtered ions could not densely agglomerate on the substrate [27, 47-48]. However, for TON-20 and TON-25 films with longer sputtering time, more grain agglomerations occurred on the substrates to form a denser film layer. Representative photomicrographs for the films (TON-10 and TON-25) are shown in Figs. 8(a) and (d) respectively. The images for samples deposited at lower deposition time are shown to be composed largely of dispersed particles. Meanwhile, for high sputtering time, distinct changes are observed in the surface morphologies. Larger grains

grew from coalescence of crystals and are densely populated on the substrates. Formation of denser microstructure at higher sputtering time accounted for the increase in crystallographic intensity.
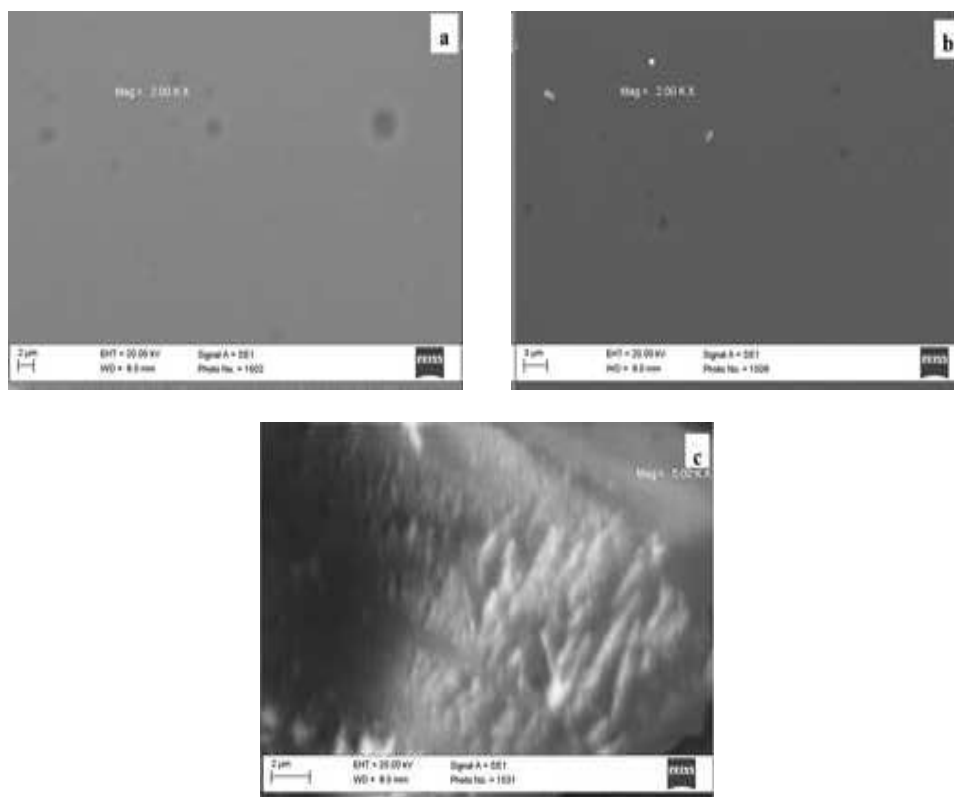

Fig. 7. Representative SEM images of TiOxNy thin films sputtered on glass substrates at (a) 5, (b) 10 and (c) 20 minutes.
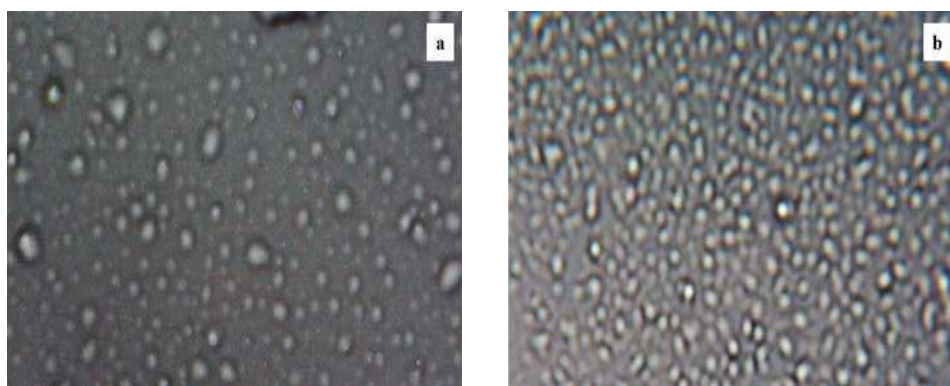

Fig. 8. Optical micrograph of the films on glass substrates (a) TON-10 and (b) TON-25.

4. Conclusions

TiNx-Oy thin films with linear thickness ranging from 243.10 to 1151.59 nm were deposited on glass substrates by direct current reactive magnetron sputtering. Using ion beam analysis, information about the thickness, stoichiometry, compositional ratio of the films was obtained. The increase in N/Ti and N/O ratios with thickness indicated transition of the sputtered films from oxynitride (TiNx-Oy) to sub-stoichiometric nitride (Ti$_2$N-O) characteristics. Structural evolution of the thin films was observed, with increase in crystalline phase peak intensity and

crystallite size with thickness. The preferred orientation of the crystalline phase at plane (111) is attributed to α-Ti. The optical properties of the films were not only influenced by the thickness, but also by the stoichiometry. The energy bandgap for the films decreased from 3.72 to 2.81 eV with thickness. The bandgap variation agrees well with the observed stoichiometric and structural properties of the films. At the sputtering pressure condition adopted, with increase in deposition time, TiNx-Oy thin films with stoichiometry and optical features ranging from non-metallic (oxynitride) to nitride with metallic features were obtained.

Acknowledgement

References

[1] M. J. Jung, K. H. Nam, Y. M. Chung, J. H. Boo, J. G. Han, Surf. Coat. Tech. 171 (2002).

[2] F. Vaz, P. Cerqueira, L. Rebouta, S. M. C. Nascimento, E. Alves, P. Goudeau, J. P. Riviere, K. Pischow, J. D. Rijk, Thin Solid Films 447 (2004).

[3] J. Pelleg, L. Zevin, S. Lungo, N. Croitoru, Thin Solid Films 197 (1991).

[4] E. Martínez- Ferrero, Y. Sakatani, C. Boissière, D. Grosso, A. Fuertes, J. Fraxedas, C. Sanchez, Adv. Funct. Mater. 17 (2007).

[5] F. Chen, S.-W. Wang, L. Yu, X. Chen, W. Lu, Opt. Mater. Exp. 4 (2014).

[6] J. Zhang, T. P. Chen, X. D. Li, Y. C. Liu, Y. Liu, H. Y. Yang, Opt. Mater. Express 6 (2016).

[7] A. Yoshikawa, "Development and Applications of Wide Bandgap Semiconductors," in Wide Bandgap Semiconductors, Springer 2 (2007).

[8] S.-C. Shen, "Wide-bandgap device research and development at SRL," Georgia Institute of Technology, 2014.

[9] T. Ludtke, A. Schmidt, C. Gobel, A. Fischer, N. Becker, C. Reimann, T. Bredow, R. Dronskowski, M. Lerch, Inorg. Chem. 53 (2014).

[10] Y. Yea, R. Lim, J. M. White, J. Appl. Phys. 106 (2009).

[11] G. Hitoki, T. Takata, J. N. Kondo, M. Hara, H. Kobayashiand, K. Dome, Chem. Commun. 16 (2002).

[12] J. M. Chappe, J. Gavoille, N. Martin, J. Lintymer, J. Takadoum, J. Mater. Sci. 41 (2006).

[13] A. Rizzo, M. A. Signore, L. Mirenghi, T. Di Luccio, Thin Solid Films 517 (2009).

[14] L. Braic, N. Vasilantonakis, A. Mihai, I. J. Villar-Garcia, S. Fearn, B. Zou, N. M. Alford, B. Doiron, R. F. Oulton, S. A. Maier, A. V. Zayats, P. K. Petrov, Appl. Mater. Interfaces. 9 (2017).

[15] R. Chandra, A. K. Chawla, D. Kaur, P. Ayyub, Nanotechnology. 16 (2005).

[16] M. H. Kazemeini, A. A. Berezin, N. Fukuhara, Thin Solid Films. 372 (2000).

[17] J. Graciani, J. Fdez Sanz, T. Asaki, K. Nakamura, J. Rodriguez, Process. J. Chem. Phys. 126 (2007).

[18] C. Rousselot, N. Martin, Surf. Coat. Tech. 142–144 (2001).

[19] N. Martin, O. Banakh, A. M. E. Santo, S. Springer, R. Sanjines, J. Takadoum, F. Levy, Appl. Surf. Sci. 185 (2001).

[20] J.-M. Chappe, N. Martin, J. Lintymer, F. Sthal, G. Terwagne, J. Takadoum, Applied Surface Science. 253 (2007).

[21] F. Vaz, P. Cerqueira, L. Rebouta, S. M. C. Nascimento, E. Alves, P. Goudeau, J. P. Riviere, F. Ribeiro, I. Moutinho, K. Pischow, J. D. Rijk, Surf. Coat. Technol. 191 (2005).

[22] B. Soundiraraju, B. K. George: ACS Nano.11 (2017) 8892. DOI:10.1021/acsnano.7B03129

[23] Pierre Villars, "PAULING FILE in: Inorganic Solid Phases, Springer Materials (online database) Ti2N Crystal Structure," Springer, Heidelberg, (2016).

[24] N. Döbelin, R. Kleeberg, J. Appl. Cryst. 48 (2015).

[25] M. Mayer, "SIMNRA version 6.06," Max-Planck-Institut fur Plasmaphysik, Garching, Germany, (2006). www.rzg.mpg.de/~mam.

[26] G. V. Naik, J. L. Schroeder, X. Ni, A. V. Kildishev, T. D. Sands, A. Boltasseva, Opt. Mater. Express. 2 (2012).

[27] E. Ajenifuja, G. A. Osinkolu, A. Y. Fasasi, D. A. Pelemo, E. I. Obiajunwa, J Mater Sci: Mater Electron. 27 (2016).

[28] E. Ajenifuja, A. P. I. Popoola, O. Popoola, J. Mater. Res. Technol. (2018).

[29] D. Mao, K. Tao, J. Hopwood, J. Vac. Sci. Technol. A. 20 (2001).

[30] E. Ajenifuja, A. Y. Fasasi, G. A. Osinkolu: T. Indian Ceram. Soc. 71 (2012).

[31] Z. Ji-Cheng, L. Di-Tian, L. You-Zhen, L. Zheng, Trans. Nonferrous Met. Soc. China. 19 (2009).

[32] V. M. Fedirko, I. M. Pohrelyuk, Nitriding of Titanium and its Alloys, Kiev: Naukova Dumka, (1995).

[33] I. M. Pohrelyuk, V. M. Fedirko, O. I. Yas'kiv, D.-B. Lee, O. V. Tkachuk, C. Li, Mater. Sci. 45 (2009).

[34] W. K. Chu, J. W. Mayer, M. A. Nicholet, Backscattering Spectroscopy, London: Academic Press, (1978).

[35] J. Xiao, Y. Li, A. Jiang, J. Mater. Sci. Technol. 27 (2011)

[36] J. Tauc, Amorphous and Liquid Semiconductor, New York: Plenium Press, (1974) 159.

[37] A. K. Jonscher, Thin Solid Films. 1 (1967).

[38] O. Özakın, B. Güzeldir, M. A. Yıldırım, M. Sağlam, A. Ateş, Phys. Status Solidi A. 209 (2012).

[39] E. S. M. Goh, T. P. Chen, C. Q. Sun, Y. C. Liu, J. Appl. Phys. 107 (2010).

[40] N. S. Das, P. K. Ghosh, M. K. Mitra, K. K. Chattopadhyay, Physica E. 42 (2010).

[41] K. O. Oyedotun, E. Ajenifuja, B. Olofinjana, B. A. Taleatu, E. Omotoso, M. A. Eleruja, E. O. B. Ajayi, Materials Science-Poland. 33 (2015).

[42] H.-S. Moon, K.-S. Ji, J.-W. Park: J. Korean Phys. Soc. 40 (2002).

[43] S. F. Glavatskikh, A. I. Gorshkov: Doklady Akademii Nauk SSSR. 327 (1992).

[44] R. W. G. Wyckoff, "Hexagonal closest packed, hcp, structure," in Crystal Structures, 2nd ed., New York, New York: Interscience, (1963) 7 - 83.

[45] R. M. Wood, Proc. Phys. Soc. 80 (1962).

[46] A. E. Adeoye, E. Ajenifuja, B. A. Taleatu, Y. A. Fasasi, Journal of Materials. 2015 (2015).

[47] V. Chawla, R. Jayaganthan and C. Ramesh, J. Mater. Sci. Technol. 26 (2010).

[48] L. I. Maissel and R. Glang, Handbook of Thin Film Technology, New York: McGraw-Hill, (1970) 1.